Fluorescein Excited-State Proton Exchange Reactions: Nanosecond Emission Kinetics and Correlation with Steady-State Fluorescence Intensity

Jose M. Alvarez-Pez,* Luis Ballesteros, Eva Talavera, and Juan Yguerabide

Department of Physical Chemistry, University of Granada, Cartuja Campus, Granada 18071, Spain

Received: January 30, 2001; In Final Form: April 11, 2001

Fluorescein is a complex fluorophore that can exist in one or more of four different prototropic forms (cation, neutral, dianion, and monoanion) depending on pH. In the pH range 6–10, only the dianion and monanion forms are important. In a previous article, we showed by steady-state fluorescein measurements that an excited fluorescein molecule displays excited-state proton transfer reactions which interconvert the monoanion and dianion forms. However, we found that these reactions can occur only in the presence of a suitable proton donor–acceptor buffer such as phosphate buffer. Assuming that, at 1 M phosphate buffer concentration, the excited-state proton exchange reaction of fluorescein rapidly equilibrates during the lifetime of fluorescein, we were able to fit quantitatively steady-state fluorescence intensity vs pH titration graphs to a relatively simple reaction model. In this article, we use nanosecond emission (decay time) methods to study the excited-state proton reactions of fluorescein in the pH range 6–10 and in the presence of a phosphate buffer concentration. Fluorescein is a challenging fluorophore for the study of excited-state proton reactions because of the strong overlap of the absorption and emission spectra of the monoanion and dianion forms of fluorescein. However by recording nanosecond emission graphs and using methods of analysis of high precision, we have been able to test kinetic mechanisms and evaluate the specific rate constants for the excited-state proton reactions as well as the lifetimes of the monoanion and dianion. Using these values for lifetimes and rate constants, we discuss the process of equilibration in the excited-state and derive expressions which allow us to predict how quickly the excited-state reactions can reach equilibrium. Moreover, we use the above kinetic and spectral parameters to calculate steady-state fluorescence intensity F_S vs pH at 1 M phosphate buffer concentration and compare this theoretically calculated graph with the experimental graph.

Introduction

Fluorescein is a complex molecule that in solution can exist in four prototropic forms (cation, neutral, monoanion, and dianion) in the pH range 1–10.[1] In the ground state these forms are in equilibrium with each other and can be detected by optical absorption spectral measurements. At any pH, the concentrations of the different fluorescein prototropic forms can be predicted from equilibrium theory and from the pK_a values for these different species (cation, $pK_C = 2.19$; neutral, $pK_N = 4.4$; and monoanion, $pK_M = 6.36$). The titration graph of optical absorbance at a given wavelength vs pH for fluorescein can be predicted from the concentrations of the prototropic forms vs pH and their molar decadic extinction coefficients ϵ (at $\lambda = 437$ nm; cation, $\epsilon_C = 49800$; neutral, $\epsilon_N = 12000$; monoanion, $\epsilon_M = 20700$; dianion, $\epsilon_D = 6300$ M^{-1} cm^{-1}). In the pH range 6–10, the monoanion–dianion equilibrium prevails, i.e, above pH 6 the concentrations of the cation and neutral forms are essentially zero.[2]

When a fluorescein solution is excited by a fast pulse of light, the initial concentrations of the different excited prototropic forms are not at equilibrium values because of (a) preferential excitation of one or more of the forms (depending on exciting wavelength and extinction coefficients) and (b) differences in the values of the equilibrium constants pK_a* in the excited state compared to the ground state ($pK_M^* = 6.3$). Therefore, there is

a tendency for the different excited forms to interconvert through excited-state proton reactions so as to achieve equilibrium during their lifetimes. In a previous article we showed that at low buffer concentrations (5 mM phosphate) and pH range 6–10, the excited-state monoanion–dianion proton reaction is too slow to have a significant effect on steady-state fluorescence intensity vs pH during the short lifetimes of the these anions (around 4 ns). That is, at low phosphate the excited monoanion and dianion are not coupled by the excited state proton reaction and therefore decay independently of each other. However, we found that in the presence of a suitable proton donor–acceptor, such as phosphate ions, the excited state monoanion–dianion proton transfer reaction occurs very efficiently and the decays of the excited monoanion and dianion become coupled. Specifically, we showed that phosphate buffer begins to have a noticeable effect on the steady-state fluorescence intensity vs pH titration graph at 20 mM phosphate buffer concentration and the effect increases with increase in phosphate buffer concentration. At 1 M phosphate buffer concentration, we postulated that the excited monoanion–dianion proton reaction is so fast that it quickly reaches equilibrium during the excited-state lifetimes of the anions and, on the basis of this postulate, we were able to obtain a quantitative fit to the titration graph of steady-state fluorescence intensity vs pH.[2]

In this article we examine the fluorescein excited-state anion–dianion proton exchange reaction by means of nanosecond emission (fluorescence decay) measurements at different pH's and phosphate buffer concentrations. Analysis of the decay

* To whom correspondence should be addressed. Phone: + 34-958-243831. Fax: + 34-958-244090. E-mail: jalvarez@ugr.es.

Fluorescein Excited-State Proton Exchange Reactions

J. Phys. Chem. A, Vol. 105, No. 26, 2001 **6321**

curves yields values for the monoanion and dianion lifetimes and specific rate constants (forward and reverse) for the excited-state proton-transfer reaction and their dependence on pH and phosphate buffer concentration. On the basis of lifetime data, we examine the postulate that at 1 M phosphate buffer concentration the excited-state monoanion−dianion reaction achieves rapid equilibrium during the lifetime of excited fluorescein and derive expressions which allow us to predict, from lifetimes and specific rate constants, the time required for an excited-state proton reaction to achieve equilibrium. More-over, we use the nanosecond emission data to predict lifetime data for fluorescein at different pHs and phosphate buffer concentrations as well as to calculate the steady-state fluores-cence intensity vs pH graph at 1 M phosphate buffer concentra-tion and compare the results with the corresponding experi-mental graphs.

The nanosecond emission study of the monoanion−dianion proton exchange reaction is a challenging problem because of the strong overlap of the absorption and emission spectra of the mono- and dianion and because the pK_a's of the monoan-ion−dianion reaction in the excited and ground states are very similar. Changes in pH affect both the ground and excited state reactions. Most studies of excited-state proton exchange reac-tions have been conducted with fluorophores where the absorp-tion and emission spectra of the conjugate acid and conjugate base forms of the fluorophore have only a small overlap and the pK_a's for the ground and excited states are very different so that changes in pH affects the excited state but not the ground-state reaction.[3] The complexity of the fluorescein monoanion−dianion reaction requires experimental decay graphs and meth-ods of analysis of high precision in order to evaluate lifetimes and specific rate constants.

Materials and Methods

Reagents. Sodium monobasic and dibasic phosphate, ethanol and potassium hydroxide are from Merck. Fluorescein acid yellow (free acid crystalline) is from Sigma Chemical Co. Fluorescein was purified by recrystallization with ethanol. The purified product was checked by means of fluorescence and absorption spectra as well as by thin-layer chromatography. All other chemicals were used without further purification.

Solutions. Fluorescein solutions were prepared by dissolving fluorescein in 1 mL of deionized−distilled water containing 0.1 mL of 1 M KOH. The volume of the latter solution was increased to 100 mL by the addition of water to give a 5×10^{-4} M fluorescein solution. 10^{-5} M fluorescein solutions with appropriate Na_2HPO_4 or NaH_2PO_4 concentration were prepared by dissolving Na_2HPO_4 or NaH_2PO_4 in deionized−distilled water and adding 2 mL of 5×10^{-4} M fluorescein solution. The volume was then increased to 100 mL by the addition of water to give a solution of appropriate concentration of Na_2HPO_4 or NaH_2PO_4 and 10^{-5} M fluorescein concentration. For high pH solutions, the pH was adjusted with KOH. Fluorescein solutions were kept in the dark when not in use because fluorescein deteriorates on exposure to light[4] and heat.[5]

Experimental Procedures. Absorption spectra were recorded with a Perkin-Elmer Lambda 16 UV−vis spectrophotometer with 1 cm light path cuvettes. Steady-state fluorescence spectra were recorded on a Shimadzu RF5001 spectrofluorometer operating in the L format with a thermostated cell holder using 1 cm light path cuvettes. Nanosecond emission was recorded with an Edinburgh Analytical Instrument FL900 ns spectrof-luorometer operating in the time-correlated single photon counting mode (TCSPC). Fluorescence lifetime data were obtained with a free running discharge flashlamp (nF900 Nanosecond Flashlamp) operating at 7.0 kV, 0.40 bar, and a frequency of 40 kHz. The decay profiles were collected over 1024 channels of the multichannel analyzer with a time-per-channel of 0.048 ns until 10^4 counts were collected in the peak channel. The instrument response function (IRF) was measured with a light scattering solution (LUDOX Colloidal silica, Sigma) in the sample compartment. For each sample, the IRF was recorded before and after recording the sample nanosecond emission graph collection (10^4 counts in the peak channel) to ensure the stability of the instrument and lamp. The IRF and decay profiles were collected with a bandwidth of 7 nm for both the excitation and emission monochromators. The IRF did not change appreciably from the first to the last sample as required for precise analysis of nanosecond emission graphs by the global analysis method.

Experimental decay curves were analyzed by means of the following convolution integral:[6]

$$F(t) = \int_0^t L(t - t')I(t')\mathrm{d}t' \tag{1}$$

where $F(t)$ is the experimentally measured decay curve, $L(t)$ is the time profile of the exciting light pulse, and $I(t)$ is the law of decay of the sample when excited by an instantaneous pulse of light. We assume that $I(t)$ can be expressed as a sum of n exponential functions with n lifetimes as shown in the following expression.

$$I(t) = A + \sum_1^n \alpha_i\, e^{-(t+\delta t)/\tau_i} \tag{2}$$

where τ_i is the ith lifetime, α_i is the preexponential or weighting coefficient, A is a background term, and δt is a temporal shift term. The temporal shift δt is used to compensate for a small time shift in the leading edge of the decay curve, relative to the recorded lamp time profile, due to differences in the wavelengths of the emission and excitation wavelengths. Equations 1 and 2 were curve fitted to the different experimental $F(t)$ vs t graphs by nonlinear least-squares analysis using the Marquardt algo-rithm.[7]

To increase the precision of the analysis of our $F(t)$ graphs, we have employed the method of "global" analysis in which more than one fluorescence decay graph is used simultaneously in the nonlinear analysis with eqs 1 and 2.[8] This method of analysis significantly increases the reliability of the evaluated weighting coefficients and lifetimes. In general, we collect six decay profiles for each fluorescein sample (at a specific pH and phosphate buffer concentration). Since the six decay profiles form a family of graphs with the same lifetimes and weighting coefficients, τ_i and α_i are linked within the set of decay graphs. The best fitting parameters were determined by minimizing the global reduced χ^2_g.[8]

Theory of Excited State Proton Transfer Reactions

The reaction scheme for excited-state proton transfer in the presence of a proton acceptor such as phosphate is shown in Figure 1. A and B refer to the conjugate acid and conjugate base forms of the fluorophore, respectively. When applied to fluorescein, A is the monoanion M and B is the dianion D. RH and R refer, respectively, to the proton donor and acceptor (for phosphate buffer, $H_2PO_4^-$ is the proton donor and $HPO_4^=$ is the proton acceptor in the pH range 6−10).

In Figure 1, the ground state species B can reversibly react with RH to form ground-state species A. The excited species
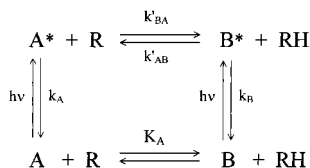
Figure 1. Kinetic scheme of ground and excited-state proton exchange reactions. A and B are ground-state conjugate acid and base forms of the fluorophore and A* and B* are excited species.

A* and B* can participate in a variety of reactions which include reaction with RH or R and return to the ground state by fluorescence (F), internal conversion (IC) and intersystem crossing (ISC). In Figure 1, we combine the latter rate constants into the total rate constants k_A and k_B defined as $k_A = (k_{FA} + k_{ICA} + k_{ISCA})$ and $k_B = (k_{FB} + k_{ICB} + k_{ISCB})$. The second-order rate constant describing the reaction B* + RH → A* + R is represented by k'_{AB}, and the second-order rate constant for the reverse reaction is represented by k'_{BA}. Although we have experimental evidence which shows that the excited monoanion−dianion proton reaction does not occur significantly in the absence of phosphate buffer, we nevertheless, for generality, also include the unaided reversible reaction A* ⇌ B* + H⁺ (not shown in Figure 1 but included in the following rate equations). We denote the first-order rate constant for the dissociation of A* into B* and H⁺ by k_{BA} and the bimolecular rate constant for the reverse reaction by k_{AB}.

For the reaction scheme of Figure 1, the solution of the coupled differential rate equations are the well-known biexponential expressions:[9]

$$[B^*] = \beta_{BS} e^{\gamma_S t} + \beta_{BL} e^{\gamma_L t} \qquad (3)$$

$$[A^*] = \beta_{AS} e^{\gamma_S t} + \beta_{AL} e^{\gamma_L t} \qquad (4)$$

where

$$\gamma_{S,L} = \frac{-(a + c) \mp \sqrt{(c - a)^2 + 4bd}}{2} \qquad (5)$$

and $a = k_A + k_{BA} + k'_{BA}[R]$; $b = k_{AB}[H^+] + k'_{AB}[RH]$; $c = k_B + k_{AB}[H^+] + k'_{AB}[RH]$; $d = k_{BA} + k'_{BA}[R]$. [R] and [RH] are related to total buffer concentration, $C_{RH} = [R] + [RH]$, by the expressions $[RH] = C_{RH}[H^+]/([H^+] + K_{RH})$ and $[R] = C_{RH} K_{RH}/([H^+] + K_{RH})$ where K_{RH} is the dissociation constant for reversible reaction RH ⇌ R + H⁺.

The γ factors are related to the lifetimes τ_S and τ_L by the expression

$$\tau_{S,L} = -\frac{1}{\gamma_{S,L}} \qquad (6)$$

where S and L refer to short and long lifetimes.

The overlap between the absorption spectra of the fluorescein monoanion and dianion results in the direct excitation of both A and B at time zero by the δ-pulse of light. Using the initial concentrations $[A^*]_0$ and $[B^*]_0$ produced by the light pulse as initial conditions, we obtain the following expression for the four preexponential factors or weighting coefficients of eqs 3 and 4.

$$\beta_{BS} = \frac{[B^*]_0(c + \gamma_L) - d[A^*]_0}{\gamma_L - \gamma_S} \qquad (7)$$

$$\beta_{BL} = -\frac{[B^*]_0(c + \gamma_S) - d[A^*]_0}{\gamma_L - \gamma_S} \qquad (8)$$

$$\beta_{AS} = \frac{[A^*]_0(a + \gamma_L) - b[B^*]_0}{\gamma_L - \gamma_S} \qquad (9)$$

$$\beta_{AL} = -\frac{[A^*]_0(a + \gamma_S) - b[B^*]_0}{\gamma_L - \gamma_S} \qquad (10)$$

The decay of fluorescence intensity following excitation of a fluorescein solution by a δ-pulse of light is given by the expression

$$I(t) = \kappa(k_{FB}(\lambda_{em})[B^*] + k_{FA}(\lambda_{em})[A^*]) = \alpha_S e^{\gamma_S t} + \alpha_L e^{\gamma_L t} \qquad (11)$$

where $k_{FA}(\lambda_{em})$ and $k_{FB}(\lambda_{em})$ are the emission rate constants at the experimental λ_{em} for A* and B*, and κ is an instrumental factor. Substituting β_{ij} into eqs 3 and 4, and then into eq 11, we obtain the following relations between kinetic rate constants (and related parameters) and the weighting coefficients:

$$\alpha_S = \frac{\kappa \epsilon_A C_t}{\gamma_L - \gamma_S} \times$$
$$[k_{FB}(\lambda_{em})\{\epsilon_R K_A(c + \gamma_L) - d[H^+]\} + k_{FA}(\lambda_{em})\{[H^+](a + \gamma_L) - bK_A \epsilon_R\}]/[K_A + [H^+]] \quad (12)$$

$$\alpha_L = -\frac{\kappa \epsilon_A C_t}{\gamma_L - \gamma_S} \times$$
$$[k_{FB}(\lambda_{em})\{\epsilon_R K_A(c + \gamma_S) - d[H^+]\} + k_{FA}(\lambda_{em})\{[H^+](a + \gamma_S) - bK_A \epsilon_R\}]/[K_A + [H^+]] \quad (13)$$

where $\epsilon_R = \epsilon_B/\epsilon_A$ is the ratio of the molar decadic extinction coefficient of A and B in the ground state at λ_{ex} and C_t is the total fluorescein concentration. It should be noted that $[A^*]_0$ and $[B^*]_0$ are functions of (1) ϵ_A and ϵ_B at the excitation wavelength and (2) ground-state concentrations of A and B. In turn, the latter concentrations are functions of pH and the dissociation constant K_A for the ground-state reversible reaction A ⇌ B + H⁺.

Results and Analysis

As mentioned above, a fluorescein molecule in aqueous solution can exist as a cation, neutral, monoanion, or dianion species depending on pH. Figure 2 shows the chemical structures and ground state proton reaction of the fluorescein monoanion and dianion, the only prototropic forms significant in the pH range 6−11.

Figure 3 shows the absorption and normalized emission spectra of the fluorescein monoanion and dianion. As can be seen, the visible range absorption maximum of the dianion is at 490 nm. The monoanion has two visible range maxima, one at 440 nm and the other at 470 nm. The largest difference in the extinction coefficients of the mono- and dianion is at 420 nm. Moreover, the dianion extinction coefficient is very small at this wavelength. The emission spectra of both anion and dianion have their maxima around 515 nm. The emission efficiency is much greater for the dianion than monoanion although this is not revealed in Figure 3 since the presented emission spectra are normalized to the same peak intensity.
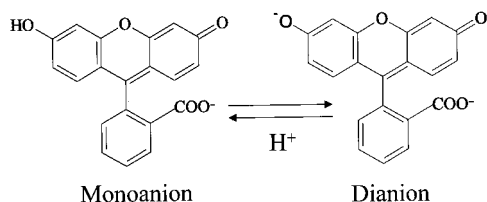
Figure 2. Chemical structures and ground-state proton reaction of the fluorescein monoanion and dianion.

We have measured nanosecond emission graphs for 10^{-5} M fluorescein at different pH's (ranging from pH 6−10) and phosphate buffer concentrations of 1 mM and 1 M. Nanosecond emission graphs were recorded at two different wavelengths, namely 420 and 440 nm. Both of these wavelengths favor the preferential excitation of the fluorescein monoanion but a significant amount of the dianion is also excited at both excitation wavelengths. Emission was detected at 515 nm ($\Delta\lambda = \pm 7$ nm) which allows efficient emission detection with minimum detection of stray incident light. Emission is dominated by the more efficiently emitting dianion species. Our choices of excitation and emission wavelengths essentially allow preferential excitation of the monoanion and detection of dianion emission, conditions that optimize the detection of the excited-state proton reactions.

For the evaluation of the lifetimes and coefficients for a fluorescein solution at a given pH and phosphate buffer concentration, we record the nanosecond emission six times (six replicates) and then analyze the resultant graphs by the global analysis, linking the lifetimes and weighting coefficients that are common to the 6 replicates. The resulting values of the lifetimes and weighting coefficients were used to calculated $F(t)$ using eqs 1 and 2 with $n = 2$. The goodness of fit of the calculated $F(t)$ to each of the replicates was evaluated by calculating the residual at each point, the global χ_g^2 and the Durbin−Watson parameter (D−W).[10]

Analysis of Lifetimes and Weighting Coefficients at Different Phosphate Buffer Concentrations. *Low Phosphate (1 mM) Buffer Concentration.* In our previous publication,[2] we found that at low phosphate buffer concentration, the excited monoanion−dianion proton-transfer reaction does not occur to any significant extent. In the present work, we find that the lifetimes and weighting coefficients which we have evaluated at low phosphate buffer concentration are consistent with this mechanism as explained in the next paragraphs.

Before discussing the experimental data at low phosphate concentration, we first consider the theory of the decay of A* and B* in the absence of excited state proton transfer reactions. In this case, A* and B* are not coupled and decay independently of each other, hence

$$I(t) = a_1 e^{-k_A t} + a_2 e^{-k_B t} \qquad (14)$$

The above equation indicates that $I(t)$ is biexponential with lifetimes τ_A and τ_B ($\tau_A = 1/k_A$ and $\tau_B = 1/k_B$). These lifetimes are independent of pH and correspond, respectively, to the lifetimes of A* and B* in the absence of excited-state proton exchange. The weighting coefficients a_1 and a_2 depend on pH. The values of a_1 and a_2 are essentially determined by the molar decadic extinction coefficients at λ_{ex} and ground-state concentrations of A and B. At a pH $\gg pK_A$, the concentration of A is insignificant, a_1 is zero, and $I(t)$ is monoexponential with a lifetime $\tau_B = 1/k_B$. That is, the lifetime at high pH is the lifetime of B* (excited fluorescein dianion). At values of pH comparable to pK_A, both a_1 and a_2 have finite values. The dependence of

the values of a_1 and a_2 on the ground state concentrations of A and B is completely determined by pH and the pK_A of the ground reaction as indicated by the Henderson−Hasselbalch equation.

We now consider to what extent the decay graphs, at low phosphate buffer concentration, correlate with the theory presented above. Figure 4A shows our experimental values of τ_S and τ_L for different pH's and 1 mM phosphate buffer concentration. Within experimental error, τ_S and τ_L are independent of pH in the pH range 6 to 10.7, as expected in the absence of excited-state proton reactions. The average values for these lifetimes are 3.69 ± 0.16 ns and 4.32 ± 0.15 ns, respectively. In the pH range 7.7 to 10.7, $I(t)$ is monoexponential with τ around 4.32 ns. In this pH range (pH $\gg pK_M = 6.36$), the monoanion concentration is insignificant. The single lifetime displayed at high pH is therefore the fluorescein dianion lifetime ($\tau_D = 4.32 \pm 0.15$ ns) which correlates well with the dianion lifetime obtained by other authors.[11] The smaller lifetime displayed at pH around 6 corresponds to the lifetime of the fluorescein monanion and we can thus write $\tau_M = 3.69 \pm 0.16$ ns.

High Phosphate Buffer. Figure 4B gives values of lifetimes for different values of pH and 1 M phosphate buffer concentration. The decay of fluorescence intensity $I(t)$ is biexponential in the pH range 5.9−7.7 and, in contrast to the low phosphate buffer case, the lifetimes are pH dependent as shown in Figure 4B. Furthermore, the weighting coefficients are opposite in sign as shown in Figure 5. All of these results are indicative of excited-state proton reactions and support the idea that such reactions are displayed by fluorescein in the presence of a suitable proton donor−acceptor. In the following sections we evaluate kinetic parameters from the data in Figure 4.

Evaluation of Kinetic Parameters from Lifetimes at High Phosphate Buffer Concentration. Laws and Brand[3] have studied the excited-state proton reaction of 2-naphthol/2-naphtholate which occurs in the absence of buffers and have suggested that k_{BA}, k'_{BA}, and k'_{AB} can be evaluated from the slope of a linear plot of $(\gamma_L + \gamma_S)$ vs pH in the absence of buffer or [R] or [RH] in the presence of buffer. From eq 5 we can write

$$\gamma_L + \gamma_S = -(a + c) = -(k_A + k_{BA} + k'_{BA}[R] + k_B + k_{AB}[H^+] + k'_{AB}[RH]) \quad (15)$$

This equation shows that, in the absence of buffer, $(\gamma_L + \gamma_S)$ vs pH gives a linear plot, but in the presence of buffer, the nonlinear dependence of [RH] and [R] on pH results in a nonlinear plot.

Instead of attempting to evaluate kinetic parameters from slopes and intercepts of linear plots, we have evaluated these parameters by nonlinear curve fit of eq 5 to the plots of τ_L and τ_S vs pH in Figure 4 (1 mM and 1 M phosphate buffer) with $\gamma_L = -1/\tau_L$ and $\gamma_S = -1/\tau_S$. The curve fit requires the evaluation of best-fitting values for six parameters, namely, k'_{BA}, k'_{AB}, k_{BA}, τ_D, τ_M, and pK_P, where the latter is pK for the phosphate buffer equilibrium $H_2PO_4^- \rightleftharpoons HPO_4^= + H^+$. (We have not included k_{AB} in our analysis for the following reasons. The maximun value for k_{AB} is around 10^{12} M^{-1} s^{-1} (diffusion-limited value). Multiplying this value by 10^{-7} (average concentration of [H$^+$] in our experiments) gives a value about 10^5 for $k_{AB}[H^+]$. The latter value is insignificant compared with the values for k'_{BA}, k'_{AB}, and k_{BA}). In the curve fitting process, we used the starting values $\tau_D = 4.32$ ns and $\tau_M = 3.69$ ns, and k'_{BA}, k'_{AB}, k_{BA} each equal to 10^9. However, we found that the end result is independent of the initial values of these parameters. The values

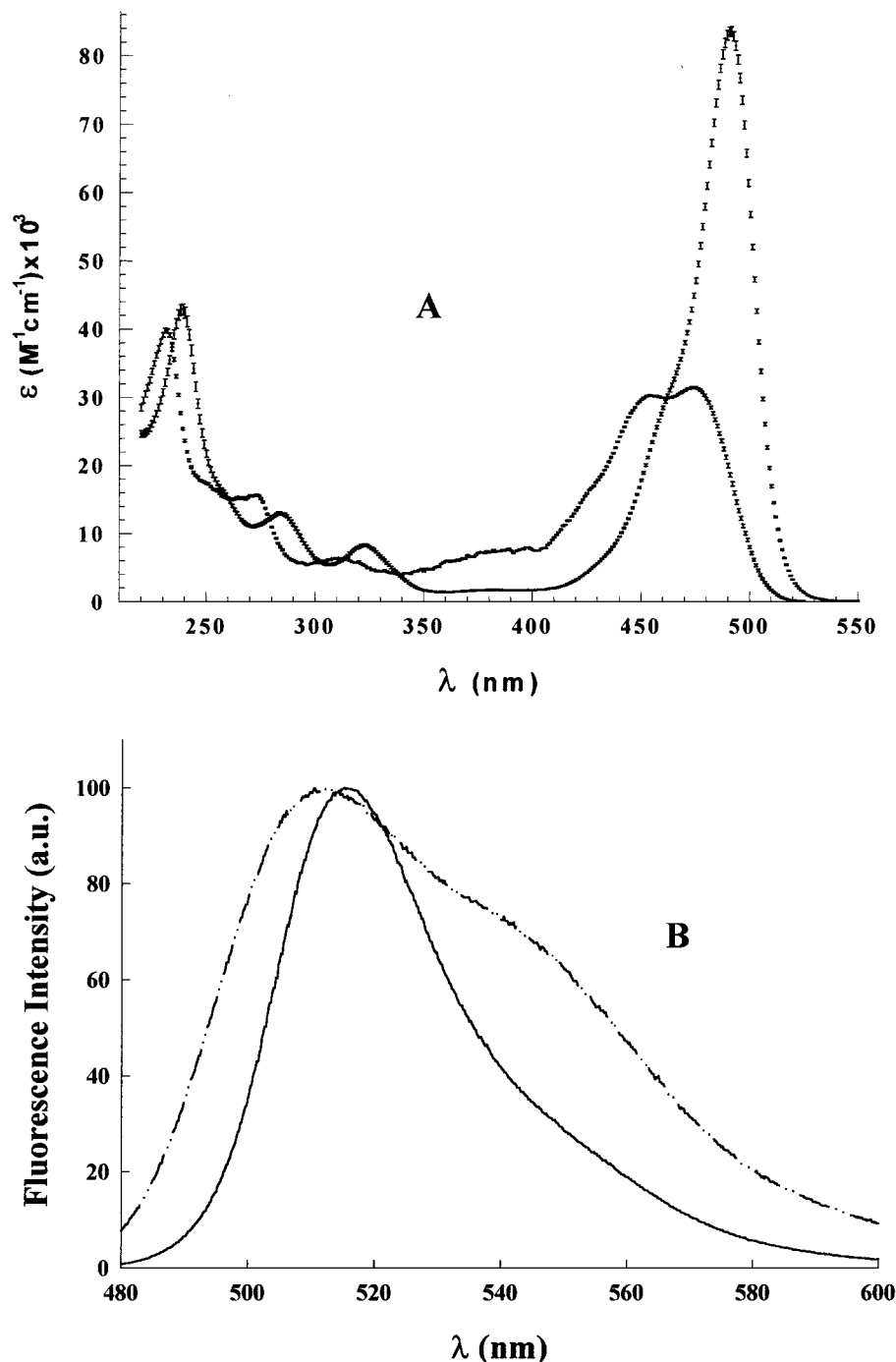**6324** *J. Phys. Chem. A, Vol. 105, No. 26, 2001*

Alvarez-Pez et al.

Figure 3. Absorption (A) and normalized emission (B) spectra of fluorescein monoanion and dianion. The extinction coefficient vs wavelength graphs were obtained by methods described in our previous publication.[2] To measure the emission spectra of the (—) dianion and (— ··) monoanion, we recorded fluorescence spectra at pH 11 (λ_{ex} = 490 nm) and pH 5.0 (λ_{ex} = 440 nm). These spectra correspond respectively to the dianion and monoanion. The spectra were normalized to have the same value at the emission maxima.

that we obtained from the nonlinear fit for the lifetimes and rate constants are shown in Table 1. The confidential interval is the asymptotic standard error (± error). The recovered τ_D and τ_M values agree, within experimental error, with the corresponding obtained from low phosphate buffer concentration. The solid curves drawn through the experimental points in Figure 4 were calculated with eq 5 using the parameter values of Table 1. The fitting correlation coefficient, r^2 = 0.995.

To improve the model of Figure 1, we have introduced into the coupled differential equations four quenching constants, namely, k_{QBRH}, k_{QARH}, k_{QBR}, and k_{QAR} for the quenching of A* and B* by RH and R. However, the curve fitting program yielded zero values for k_{QBRH}, k_{QBR}, and k_{QAR} and a value of 1.1×10^7 for k_{QARH}. These low quenching constants may be the result of repulsion between the negatively charged fluorescein dianion and monoanion and the negatively charged phosphate ions. In view of the low quenching rate constants, we have ignored them in later calculations.

In some limited experiments, we opened the slit width of the emission monochromator to its maximum value (emission band detection width = 15 nm) and found that the evaluated lifetimes do not vary with the emission band detection width. This result is consistent and expected for the kinetic model which we have used to analyze the nanosecond emission data.
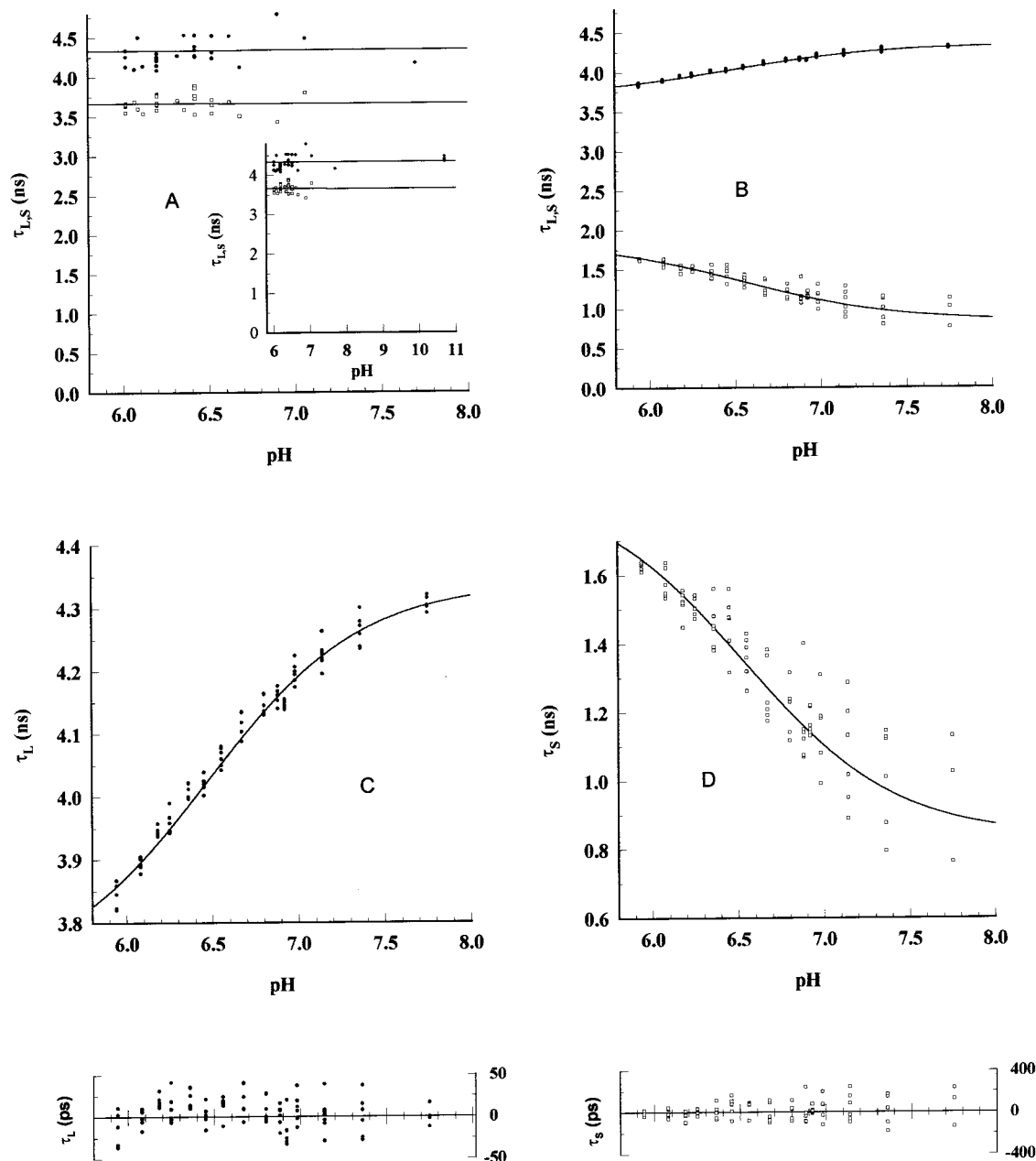
Fluorescein Excited-State Proton Exchange Reactions

J. Phys. Chem. A, Vol. 105, No. 26, 2001 **6325**

Figure 4. Graphs of τ_L and τ_S vs pH for 1 mM (A) and 1 M (B) phosphate buffer. (C) and (D) are the same as (B) but with an expanded ordinate scale. The inset is the same than (A) but the data are plotted over a larger pH range. The points in these graphs represent values obtained by deconvolution of six experimental nanosecond emission decays with linked τ_i and α_i from 10^{-5} M fluorescein solutions at different pH's. The global χ^2_g and D$-$W parameter values for all of the fittings are between 1 and 1.09, and 1.89$-$2.01, respectively. In 1 M phosphate buffer solutions each sample was analyzed three times at the two exciting wavelengths (420 and 440 nm). In 1 mM phosphate buffer solutions exciting wavelength was 420 nm. Emission wavelength was 515 nm for all of the measurements. The graphs of τ_L and τ_S in this figure were fitted to eqs 5 and 6. This fitting yielded the lifetimes and specific rate constant values shown in Table 1. The solid graphs drawn through the experimental points were calculated with eqs 5 and 6 using the values of Table 1. The graphs at the bottom of this figure represent, in picoseconds, the lifetime deviations between the experimental values and fitted lifetime vs pH.

Mechanistic Analysis of Weighting Coefficients. According to eqs 12 and 13, the weighting coefficients α_S and α_L depend on $\kappa' = \kappa\epsilon_A C_t k_{FB}(\lambda_{em})$, ϵ_R, and $k_{FR}(\lambda_{em}) = k_{FA}(\lambda_{em})/k_{FB}(\lambda_{em})$ as well as on kinetic parameters which we have already evaluated from the lifetimes in the previous section. We can thus obtain values for the nonkinetic parameters ϵ_R and $k_{FR}(\lambda_{em})$ by nonlinear curve fitting of eqs 12 and 13 to graphs of α_S and α_L vs pH using previous values for kinetic parameters and allowing the values of κ', ϵ_R, and $k_{FR}(\lambda_{em})$ to be evaluated by the nonlinear fit. However, before presenting our results of this analysis, it is necessary to discuss how we evaluate α_S and α_L from experimental nanosecond emission graphs.

Fluorescein solutions at different pH's have different inherent fluorescence intensities and these differences are reflected in the amplitudes of the nanosecond emission graphs when these graphs are recorded for the same time interval. However, when all graphs are recorded with 10000 counts in the peak, there is a loss of amplitude information and the values of the weighting coefficients obtained from these graphs cannot be related to eqs 12 and 13. It should be noted that our method for recording or accumulating nanosecond emission graphs does not affect the values of the lifetimes or the ratio of the weighting coefficients at a given pH. To obtain values of α_L and α_S that can be
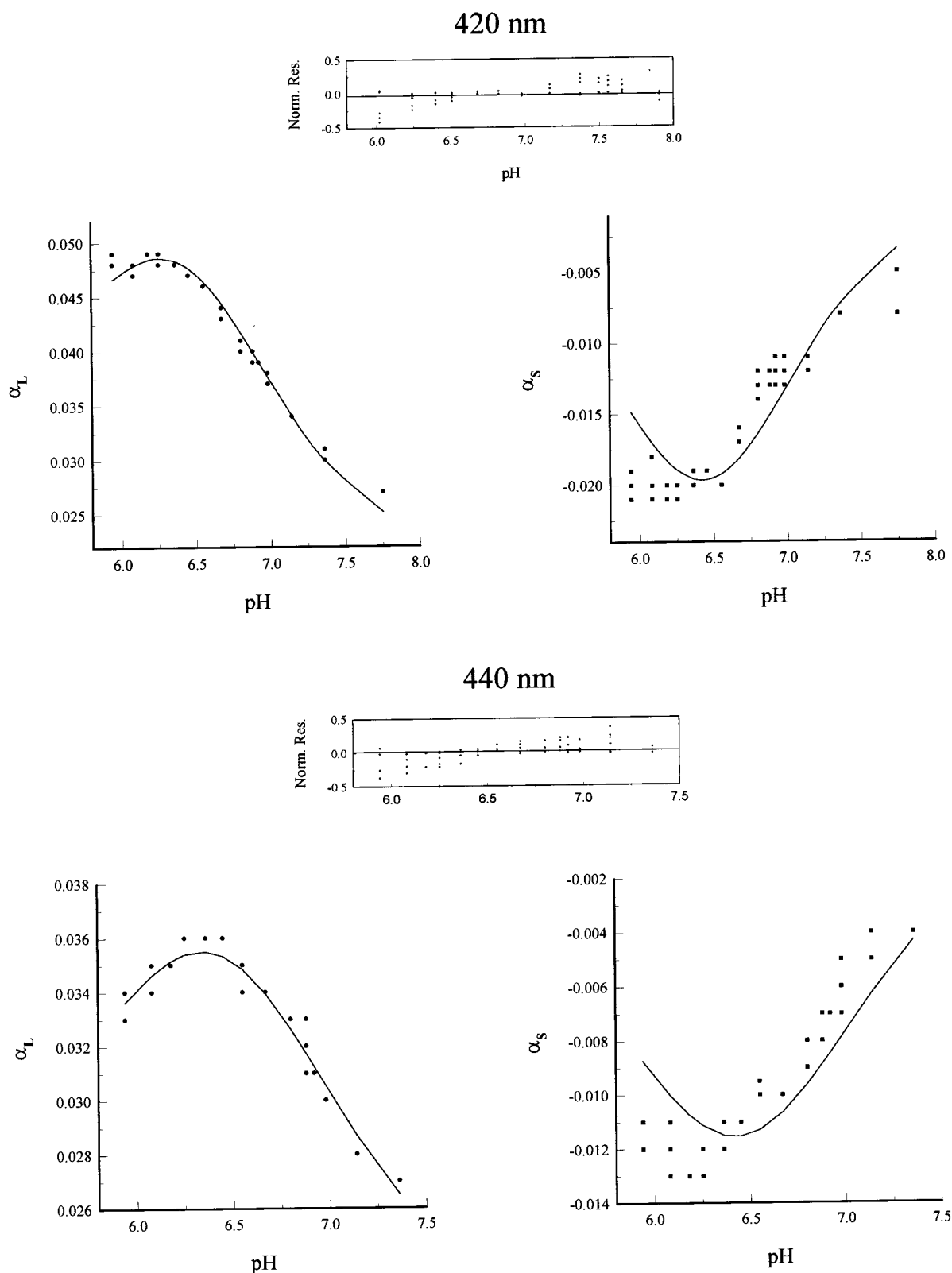
420 nm

440 nm

Figure 5. Plots of the preexponential factors α_S, α_L vs pH. The values of these parameters were obtained by global deconvolution of experimental nanosecond emission graphs whose amplitudes had been adjusted to the correct relative values. The experimental points of α_S, α_L vs pH in this figure were curve fitted to eqs 12 and 13 using the parameter values of Table 1 and allowing k_{FR}, κ', and ϵ_R to be evaluated by the curve fitting procedure. The solid curves through the experimentally derived points in this figure were calculated with eqs 12 and 13 and the parameter values of Table 1. r^2 values are 0.996 and 0.998 at 420 and 440 nm, respectively.

compared and analyzed by eqs 12 and 13 at different pH's, it is necessary to evaluate them from (1) nanosecond emission-graphs that have been recorded (accumulated) for the same time interval or (2) nanosecond emission graphs whose relative amplitudes have been adjusted so that they are equivalent to

graphs recorded for the same time interval. Drifts in lamp intensity and other instrument parameters during the long time interval needed to record several nanosecond emission graphs make it difficult to record graphs whose amplitudes have sufficient precision for the evaluation of α_S and α_L. In Appendix

TABLE 1: Kinetic Parameters Evaluated by Nonlinear Curve Fitting of Equations 5 and 6 to τ_L, τ_S, and pH Values in Figure 4 (the Curve Fits Also Yield a Value for pK_P), and Nonkinetic Parameters Evaluated by Nonlinear Curve Fitting of Eqs 12 and 13 to the Weighting Coefficients α_L and α_S of Figure 5

parameter	recovery	asymptotic std error
pK_P	6.91	0.04
τ_D (ns)	4.34	0.02
τ_M (ns)	3.70	0.03
k_{BA} (s^{-1})	2.6×10^6	1.3×10^6
k_{AB} (M^{-1} s^{-1})		
k'_{BA} (M^{-1} s^{-1})	9.2×10^8	0.4×10^8
k'_{AB} (M^{-1} s^{-1})	3.04×10^8	0.09×10^8

	$\lambda_{ex} =$ 420 nm	$\lambda_{ex} =$ 440 nm	$\lambda_{ex} =$ 420 nm	$\lambda_{ex} =$ 440 nm
k_{FR}	0.275	0.299	0.006	0.007
κ'	0.130	0.087	0.001	0.001
ϵ_R	0.167	0.251	0.004	0.005

A, we present the method which we use to obtain corrected values of α_L and α_S.

Figure 5 shows graphs of the weighting coefficients obtained from the corrected nanosecond emission graphs from 10^{-5} M fluorescein solutions at 1 M phosphate buffer concentration and different pH's, at two different exciting wavelengths. We have curve fitted these graphs with eqs 12 and 13. The best fitting values of κ', ϵ_R and $k_{FR}(\lambda_{em})$ are shown in Table 1. The values of ϵ_R are lower than the ones we previously calculated from optical absorption data ($\epsilon_R(440) = 0.397$ and $\epsilon_R(420) = 0.237$). We obtain two values of k_{FR}, for the two exciting wavelengths, which are slightly different each other.

Rate of Equilibration of Excited-State Proton Exchange Reactions. As mentioned, we have previously postulated that the excited state monoanion−dianion proton reaction of fluorescein quickly reaches equilibrium during the excited-state lifetime of fluorescein in the presence of 1 M phosphate buffer. We now examine this postulate using our present decay time results.

The fast equilibration postulate can be analyzed best using graphs of the decay of excited fluorescein dianion and monoanion at different pH's and 1 M phosphate buffer concentration. These graphs can be calculated with eqs 3−10 using values of specific rate constants and lifetimes which we have determined.

Figure 6 A−D shows nanosecond decay graphs for excited monoanion [M*] and dianion [D*] calculated with eqs 3 and 4 (M* is A*and D* is B* in these equations) for the pH range 6−8 and 1 M phosphate buffer. The calculations were done using the lifetimes and rate constants of Table 1. Graphs are shown in semilog as well as on natural scales. To check our calculations, we also calculated nanosecond emission graphs using the graphs of Figure 6 for A*(t) and B*(t) and eqs 1 and 11. We then compared the resulting graphs with experimental nanosecond emission graphs F(t). The agreement between experimental and calculated F(t) is excellent.

The attainment of equilibrium in the excited state can best be detected from plots of the ratio [D*(t)]/[M*(t)] which are shown in Figure 6E. If equilibrium is rapidly achieved between D* and M* during their lifetimes, then we expect this ratio to attain a constant value as soon as equilibrium is established. At equilibrium, the value of the ratio is determined by the equilibrium relation $[D^*(t)]_{eq}/[M^*(t)]_{eq} = K_A^*/[H^+]$ where K_A^* is the dissociation equilibrium constant for the excited-state proton reaction $M^* \rightleftharpoons D^* + H^+$ ($pK_A^* = pK_M^* = 6.3$).[2] As soon as equilibrium is established, D* and M* must decay

monoexponentially and with the same lifetime in order to maintain a constant value for the equilibrium ratio.

Examination of the graphs of Figure 6E shows that [D*(t)]/[M*(t)] vs t at the different pH's all consist of an initial rising phase followed by the equilibrium phase where the ratio is constant. In theory, the initial phase could be rising or decaying depending on the initial concentrations of M* and D* which determine which side of the excited state proton reaction is initially in excess. In the present case, M* is excited preferential so that [D*(t)]/[M*(t)] must rise in order for equilibrium to be achieved in the excited state. It should also be noted from examination of Figures 6A and B, that in the equilibrium phase, M* and D* decay exponentially with the same lifetime as expected. The above results thus indicate that at 1 M phosphate buffer concentration, the excited state proton reaction of fluorescein indeed quickly reaches equilibrium during the lifetimes of the excited mono- and dianions.

The plateaus in the equilibrium regions of the plots [D*(t)]/[M*(t)] vs t in Figure 6E correspond to $[D^*(t)]_{eq}/[M^*(t)]_{eq}$. From these ratios we can calculate pK_M^* using the Henderson−Hasselbalch equation for the excited-state equilibrium. This equation yields $pK_M^* = 6.4$ for each of the plots. This value agrees, within experimental error, with the corresponding value which we obtained from steady-state data.[2]

A more quantitative view of how fast, in general, a proton excited-state reaction achieves equilibrium can be obtained as follows. Equilibrium is achieved when the contributions of τ_S to the decay of A* and B* becomes insignificant (see Appendix B). At equilibrium A* and B* decay monotonically with a single lifetime τ_L. The times tc1 and tc2 required for the contribution of τ_S to become insignificant, respectively, for B*(t) and A*(t) are given by the following equations

$$tc1 = \frac{\ln\left|\frac{\beta_{BS}}{\beta_{BL}}\right| - \ln(\rho)}{\tau_L - \tau_S} \tau_S \tau_L \qquad (16)$$

$$tc2 = \frac{\ln\left|\frac{\beta_{AS}}{\beta_{AL}}\right| - \ln(\rho)}{\tau_L - \tau_S} \tau_S \tau_L \qquad (17)$$

where ρ is a parameter that is related to the contribution of τ_S (compared to τ_L) to the decay of B* and A* at the times tc1 and tc2. The contribution of τ_S becomes negligible for $\rho < 0.01$. Thus, with $\rho = 0.01$, or less, tc1 and tc2 are a measure of the time required to reach equilibrium.

As example of the use of the above equations we calculate β_{ij} with the parameters in Table 1 and eqs 7−10. Next we calculate tc1 and tc2 with eqs 16 and 17 for pHs in the range 6.0 to 8.0. Plots of tc1 and tc2 vs pH are shown in Figure 7. In this figure we choose the larger of the times as indicator of the time required to reach equilibrium at each pH. If we now examine Figure 6E, we see that the times (tc1 or tc2) required to reach equilibrium coincide with the times to plateau in this figure.

Lifetimes vs Phosphate Buffer Concentration at a Constant pH. From the values of the kinetic and steady-state parameters which we have obtained through analysis of the nanosecond emission data, we can predict the dependence of the lifetimes and weighting coefficients with eqs 3−13. To check these predictions we have measured experimentally the lifetimes of fluorescein solutions at pH = 6.08 for several phosphate buffer
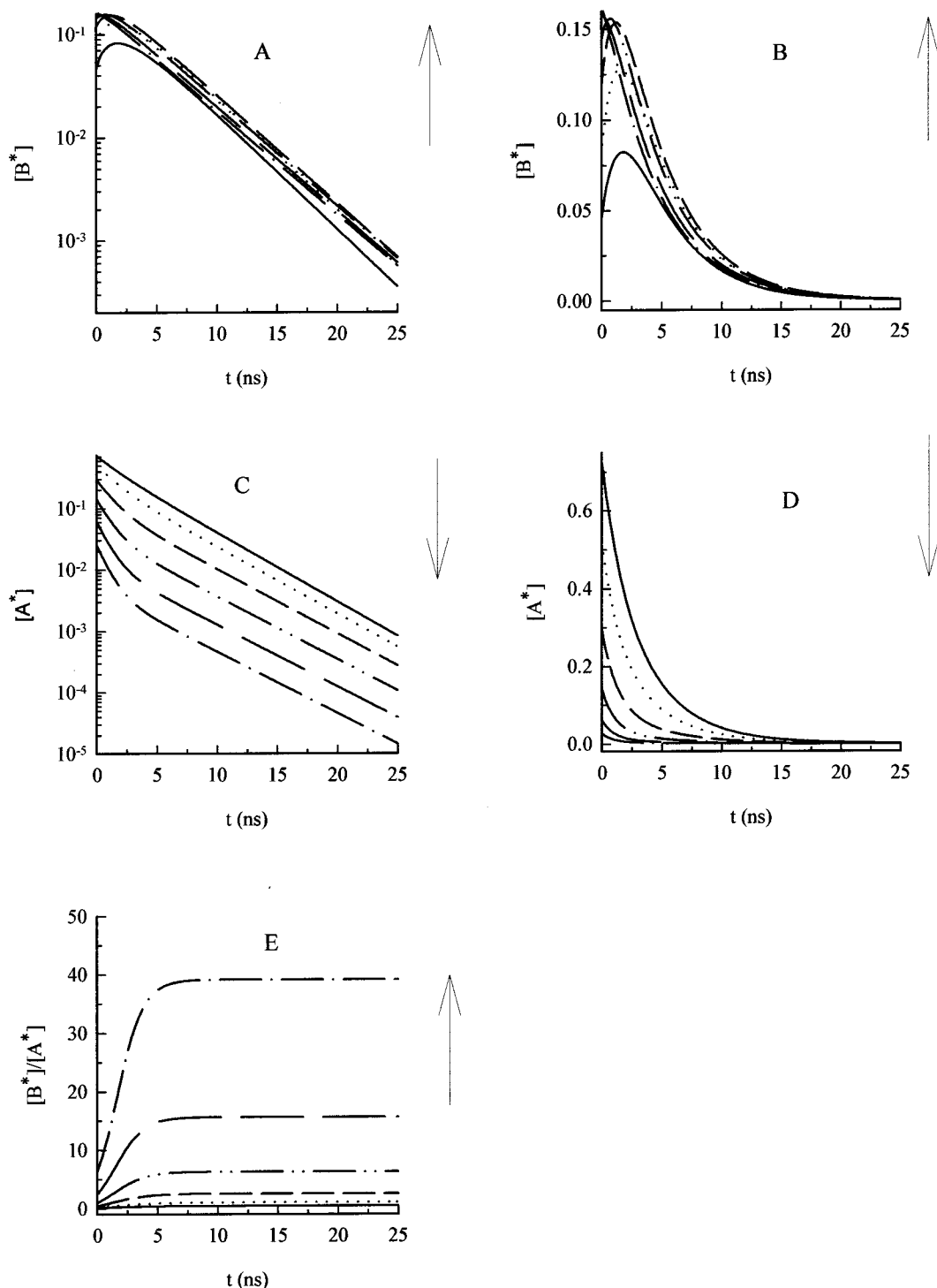
6328 *J. Phys. Chem. A, Vol. 105, No. 26, 2001*

Alvarez-Pez et al.

Figure 6. Plots of the decay of the excited monoanion A* and dianion B* of fluorescein following excitation by a fast pulse of light and different values of pH. The graphs were calculated with eqs 3–10 using the lifetimes and rate constants of Table 1 ($\lambda_{exc} = 420$ nm). The decays of A* and B* are plotted in semilog (A and C) and natural (B and D) scales. Also shown (E) is the time dependence of the ratio [B*]/[A*]. The arrows show the direction of increasing pH. The pH values are: (—) 6.0, (· ·) 6.4, (− −) 6.8, (— ··) 7.2, (−) 7.6 and (— ·) 8.0.

concentrations in the range 0.12–1.2 M. The points in Figure 8 are the experimental values for τ_S and τ_L vs phosphate buffer concentration. The solid curves are graphs calculated with eqs 5 and 6 using the kinetic parameters of Table 1. The agreement between the experimental and calculated graphs is very good.

Correlation between Nanosecond Emission and Steady-State Fluorescence Intensity. The fundamental relation between steady-state fluorescence intensity F_S and nanosecond emission (decay) $F(t)$ (after excitation by an instantaneous pulse of light)

is given by the expression

$$F_S = \chi \int_0^\infty F(t)\, dt \qquad (18)$$

This equation states that the steady-state intensity is proportional to the area under the graph of $F(t)$ vs t or the sum of all photons detected from $t = 0$ to ∞ after excitation by an instantaneous pulse of light. χ is an instrumental constant.

Fluorescein Excited-State Proton Exchange Reactions

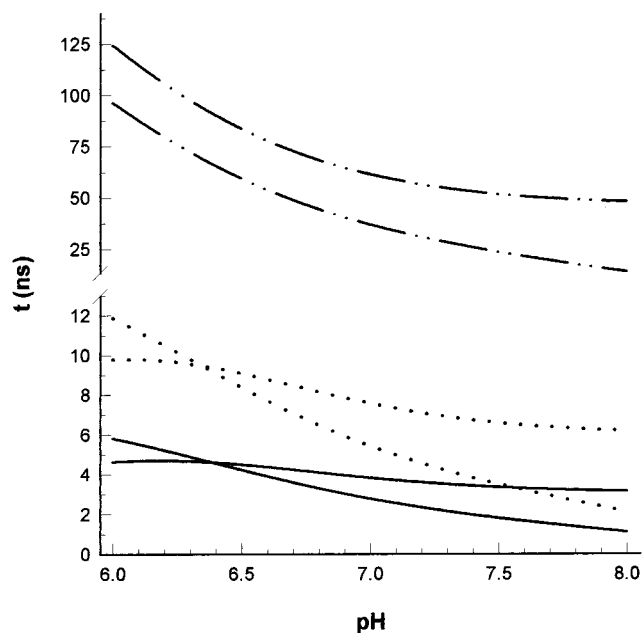*J. Phys. Chem. A, Vol. 105, No. 26, 2001* **6329**

Figure 7. Plots of the tc1 and tc2 vs pH (in the range 6.0 to 8.0), calculated with the parameters of Table 1 and eqs 5−10, 16, and 17 at different phosphate buffer concentrations: (—) 2 M, (· ·) 1 M, (— ··) 0.1 M. The larger of the times is the indicator of the time required to reach equilibrium at each pH.
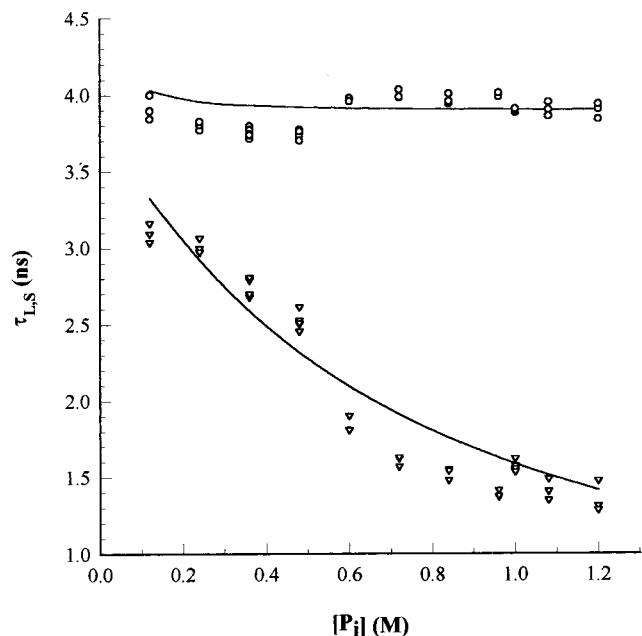

Figure 8. Experimental lifetimes vs phosphate buffer concentration at pH 6.08. The solid line drawn through the points was calculated with eqs 5 and 6 using kinetic parameter values from Table 1.

We have recorded steady-state fluorescence intensity F_S vs pH at 1 M phosphate buffer concentration using two different experimental methods. The first method is based on eq 18 and works as follows. With the nanosecond fluorometer in the single photon mode, we count all of the photons detected by the fluorometer for 10^5 excitation pulses. This number N_S is the relative value of the integral of $F(t)$ where $F(t)$ has been accumulated for 10^5 lamp pulses and we can equate it to relative steady-state fluorescence intensity of the sample. If the instrument settings are kept constant, then N_S measured for fluorescein samples at different pH's yields relative F_S vs pH. The results of these measurements are shown as discrete points in Figure

9A for λ_{exc} = 420 nm and Figure 9C for λ_{exc} = 440 nm in the pH range 6 to 8. λ_{em} is 515 nm.

We have also measured steady-state fluorescence intensity vs pH by the conventional method using a standard steady-state spectrofluorometer as described in our previous publication.[2] The results of these conventional steady fluorescence measurements are shown as discrete points in Figure 9B for λ_{exc} = 420 nm and Figure 9D for λ_{exc} = 440 nm. The conventional graphs are actually the steady-state graphs presented in our previous article. The solid curves drawn through the experimental points of Figure 9 were calculated with eqs 5−13 and 18 using the parameters values shown in Table 1.

It should be noted that although the experimentally recorded nanosecond fluorometer and conventional F_S vs pH graphs have the same form, they differ in amplitude because of different instrumental factors. Likewise, the graphs obtained directly from the theoretical calculation differ in amplitudes with respect to the experimental graphs. We have therefore normalized the graphs so that they agree in amplitudes, within experimental errors, in selected pH ranges. It can be seen that the agreement between the experimental and simulated graphs is excellent in the pH range 6 to 8.

Figure 10 shows steady-state intensity vs pH graphs over a longer pH range, pH = 6 to 11. The experimental points in the graphs of Figure 10A (λ_{exc} = 420 nm) and C (λ_{exc} = 440 nm) were obtained with the nanosecond fluorometer and those in Figure 10B (λ_{exc} = 420 nm) and D (λ_{exc} = 440 nm) with the standard steady-state fluorometer. The solid curves drawn through the experimental points are the theoretically graphs calculated as mentioned above. The theoretical graphs have been normalized so that they agree with the experimental data point at pH around 11. The agreement between the experimental and theoretical graphs is very good except in the range 8−9 where the experimental graphs display a dip that is not present in the calculated graphs. We previously reported this same discrepancy between experimental F_S vs pH graphs for fluorescein and theoretical F_S vs pH graphs which we calculated for the steady-state assuming rapid equilibration between excited fluorescein monanion and dianion at 1 M phosphate buffer.[2] As before, we believe that the dip displayed by the experimental data of Figure 10 is due to changes in the concentrations of $H_2PO_4^-$ and $HPO_4^=$ with pH in the range pH = 8−9. The pK's for the different phosphate buffer equilibria are pK_1 = 2.12 for $H_3PO_4 \rightleftarrows H_2PO_4^- + H^+$ and pK_2 = 7.2 for $H_2PO_4^- \rightleftharpoons HPO_4^= + H^+$. In the pH range above 6, the only important species are $H_2PO_4^-$ and $HPO_4^=$. Above pH 7.2, $HPO_4^=$ becomes the predominant species. The $HPO_4^=$ is apparently not as good a proton donor−acceptor as $H_2PO_4^-$.

Discussion

We have presented nanosecond emission graphs for fluorescein in solutions with different pH's and phosphate buffer concentrations and evaluated kinetic parameters for the monanion−dianion excited-state proton reaction. The evaluation of lifetimes, weighting coefficients and kinetic parameters for a complex fluorophore such as fluorescein requires nanosecond data and methods of analysis with very high precision.

Consistent with our previous results, the present results show that the fluorescein excited-state proton reaction does not occur to any significant extent during the lifetime of excited fluorescein if an adequate proton acceptor−donor is not present in the fluorescein solution. Phosphate buffer can serve as a proton donor−acceptor for the excited monoanion−dianion proton
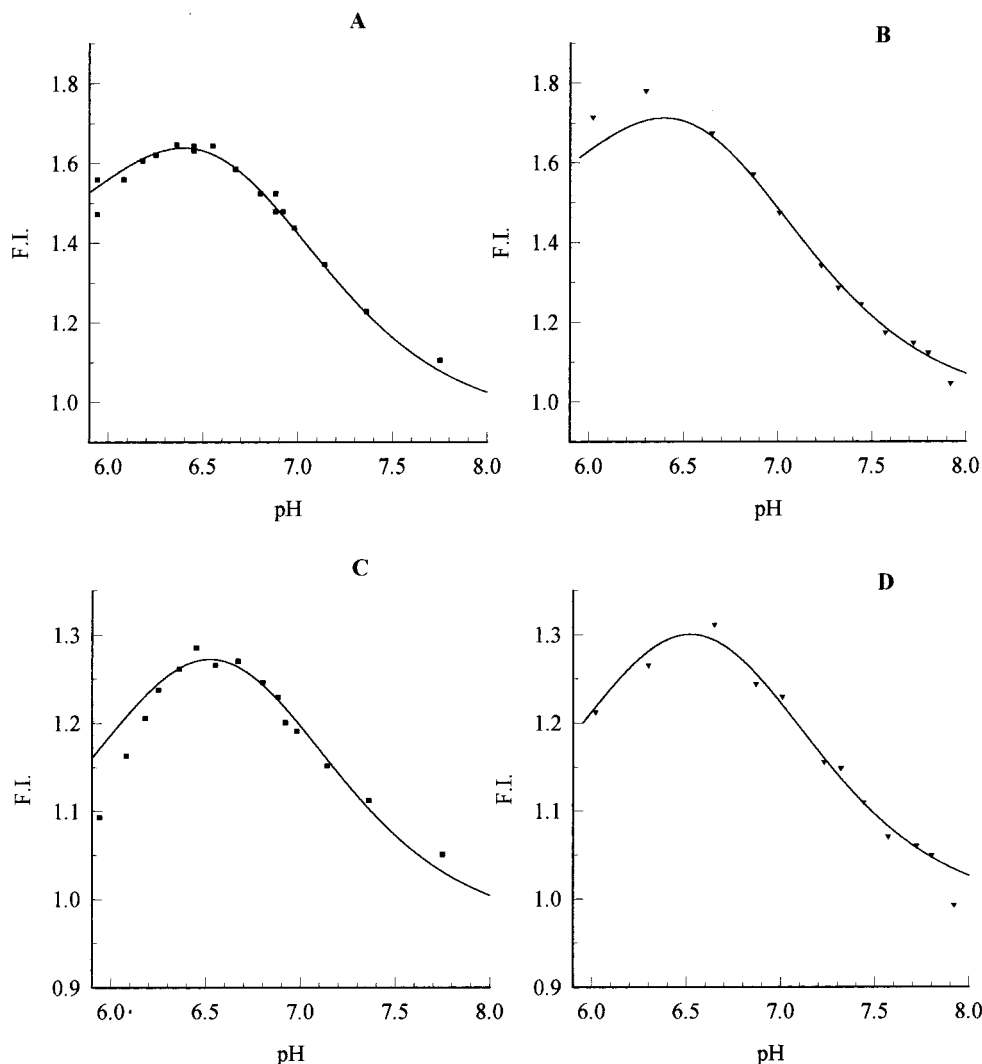
Figure 9. Graphs of steady-state fluorescence intensity F_S vs pH recorded by (1) integrating nanosecond emission data as explained in text (graphs A and C) and (2) with a conventional steady-state spectrofluorometer (graphs B and D). Graphs A and B were obtained with $\lambda_{ex} = 420$ nm and C and D with $\lambda_{ex} = 440$ nm. $\lambda_{em} = 515$ nm for all graphs. The solid graphs drawn through the experimental points were calculated with eqs 5–13 and 18 using the experimental values of parameters in Table 1. The theoretical graphs have been normalized so that they agree in amplitudes, within experimental errors, in selected pH ranges.

reaction and we have measured the rate constants for this phosphate-assisted reaction using the reaction scheme of Figure 1.

We have also used our nanosecond emission data to examine several aspects of the equilibration of the excited monoanion–dianion proton reaction in the presence of phosphate buffer. The rate at which this reaction approaches the equilibrium state is best visualized from plots of $[M^*(t)]$ and $[D^*(t)]$ vs t. We have been able to obtain these plots using theoretical expressions for $[M^*(t)]$ and $[D^*(t)]$ and values for kinetic and lifetime parameters which we obtained form analysis of nanosecond emission data. In addition, we have derived expressions which allow us to determine approximately the time tc1 or tc2 required for the excited monoanion–dianion reaction to reach equilibrium. These times can be calculated from our values of pertinent kinetic parameters.

Finally we note that the theoretical expressions which we have presented, together with the kinetic values which we have obtained from analysis of experimental decay graphs, have very high predictive power. We are for example able to calculate the excited-state behavior of the fluorescein monoanion and dianion for different phosphate buffer concentrations and pH's

in the range 6 to 10. Likewise we are able to simulate the steady-state fluorescence intensity vs pH plots.

The quantitative model and methods of analysis which we have presented apply to any reversible two-state excited-state reaction and analogous relationships can be obtained for any excited-state reaction involving excited-state complex formation, for example, excimer or exciplex formation and solvation reactions. All of these reversible reactions can be recognized by the fact that the decay graph can be represented by a biexponential function with decay times that are independent of emission wavelength and preexponential terms that are opposite in sign when excitation preferential excites one of the excited-state reactants.

Appendix A

Our method for evaluating α_L and α_S is as follows. The nanosecond emission graphs for different pH's are first each recorded with 10000 counts in the peak channel in our usual manner. Next, with the nanosecond spectrofluorometer operating
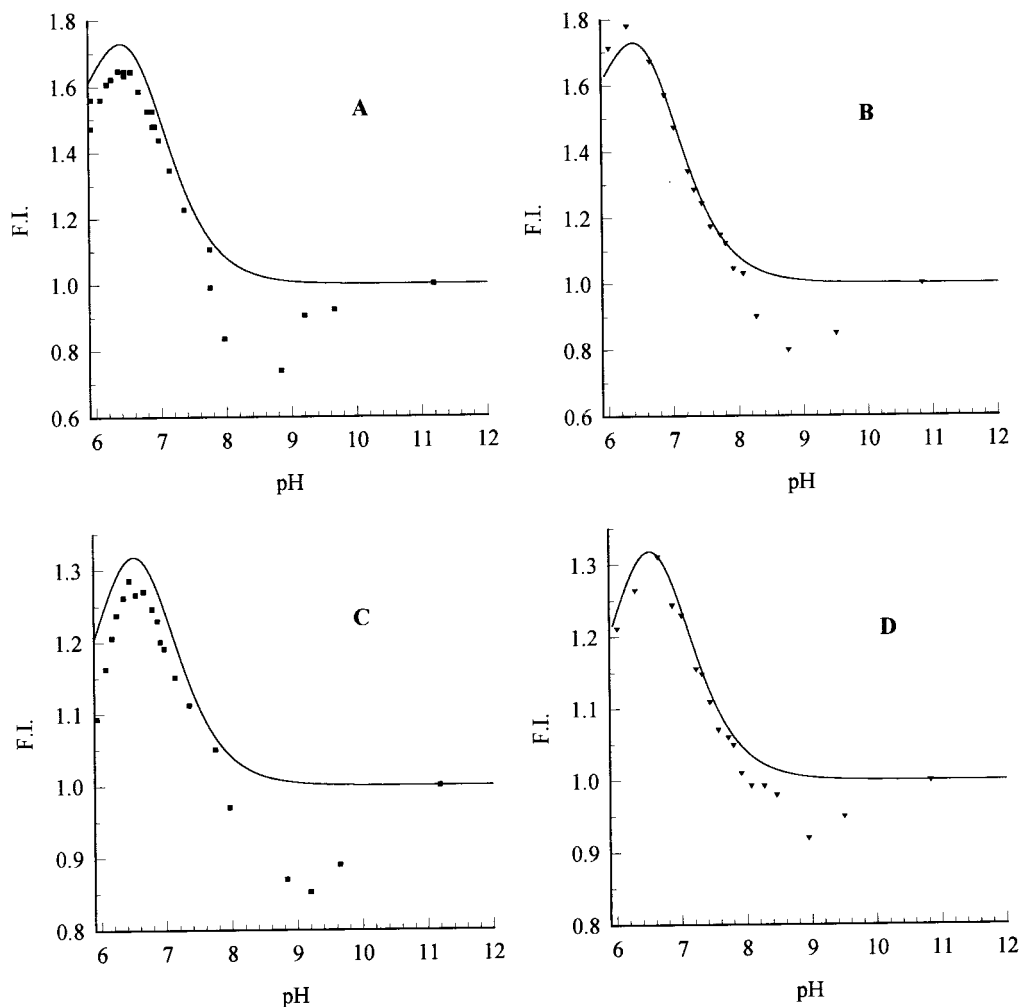
Figure 10. Same as Figure 9 but the data are plotted over a larger pH range. The theoretical graphs have been normalized so that they agree with the experimental data point at pH around 11.

in the single photon mode and with fixed instrument settings, we record for each sample the total number of photons detected by the photomultiplier tube for 10^5 lamp pulses. This total count can be obtained by (1) accumulating the nanosecond emission graph for 10^5 lamp pulses and summing the number of counts over all time channels (proportional to area of the emission graph) or (2) recording with a counter all photomultiplier single photon pulses for 10^5 lamp pulses. The total count can be obtained for all of the samples at different pH's and buffer concentrations in a short time interval (about 10 min) during which instrumental fluctuations are insignificant. The total counts recorded for the different samples are proportional to the relative areas A of the nanosecond emission graphs when recorded for the same time interval without instrument fluctuations. That is $A = \int I(t)\,dt$ where $I(t)$ is recorded for a fixed time interval. The 10000 peak count graphs can therefore be reduced to the graphs recorded for the same time interval by adjusting the areas of the graphs so that their ratios are the same as the total count ratios. This is done as follows. Let $NT(pH_i)$ represent the experimentally recorded total count for the sample at pH_i. Let $A(pH_i)$ be the area for the 10000 peak count graph where again area is defined as $\int I(t)\,dt$. Calculate the adjustment factor $C(pH_i)$ with the expression

$$C(pH_i) = \frac{NT(pH_i)}{A(pH_i)}\,F \qquad (A_A\text{-}1)$$

where F is an arbitrary factor that has the same value for all

pH's and buffer concentrations and that yields values of $C(pH_i)$ which are in a range around 1. Finally, multiply the 10000 peak count graphs by $C(pH_i)$. This multiplication yields corrected nanosecond emission graphs with the correct relative amplitudes. Weighting coefficients evaluated from the corrected graphs are directly related to eqs 12 and 13.

Appendix B

From eqs 3 and 4, we can write, in terms of lifetimes instead of γ's,

$$[B^*(t)] = \beta_{BS}\,e^{-t/\tau_S} + \beta_{BL}e^{-t/\tau_L} \qquad (A_B\text{-}1)$$

$$[A^*(t)] = \beta_{AS}\,e^{-t/\tau_S} + \beta_{AL}e^{-t/\tau_L} \qquad (A_B\text{-}2)$$

In general, B* and A* decay according to a biexponential function. However, when equilibrium is reached in the excited state, both B* and A* must decay monoexponentially with the same lifetime as discussed above. In order for this to occur, the τ_S exponential terms in the above equations must decay to practically zero compared to the τ_L exponential term. On the basis of these ideas, a general expression for calculating the time required for B* and A* to reach equilibrium can be obtained as follows. We rewrite eqs A_B-1 and A_B-2 in the following forms:

$$[B^*(t)] = \beta_{BL}\, e^{-t/\tau_L} \left(1 + \frac{\beta_{BS}}{\beta_{BL}}\, e^{-t/\tau_S} e^{t/\tau_L}\right) \qquad (A_B\text{-}3)$$

$$[A^*(t)] = \beta_{AL}\, e^{-t/\tau_L} \left(1 + \frac{\beta_{AS}}{\beta_{AL}}\, e^{-t/\tau_S} e^{t/\tau_L}\right) \qquad (A_B\text{-}4)$$

From the above equations, it is clear that the contribution of the τ_S term to the decay of A* and B* becomes insignificant when the second term in parentheses becomes much less than 1, say 0.01. If we designate this number less than 1 by the symbol ρ, then the time tc1 required for the second term in parentheses in eq A_B-3 to become insignificant can be obtained by solving the following equation for tc1.

$$\rho = \frac{\beta_{BS}}{\beta_{BL}}\, e^{-tc1/\tau_S} e^{tc1/\tau_L} \qquad (A_B\text{-}5)$$

A similar expression with tc2 can be written for A*. Solution of the above expression for tc1 gives eq 16 and similarly for tc2 gives eq 17. Note that in eqs 16 and 17 we use absolute values for the ratio of the β's because in general this ratio can have a negative sign. tc1 or tc2, which ever is larger, gives approximately (depending on the value selected for ρ) the time required for equilibrium to be established in the excited state. It should be noted that the above discussion applies to any reversible excited-state reaction, for example, excimer reactions.

References and Notes

(1) Zanker, V.; Peter, W. *Chem. Ber.* **1958**, *91*, 572.
(2) Yguerabide, J.; Talavera, E.; Alvarez, J. M.; Quintero, B. *Photochem. Photobiol.* **1994**, *60*, 435.
(3) Laws, W. R.; Brand, L. *J. Phys. Chem.* **1979**, *83*, 795.
(4) Diehl, H.; Horchak-Morris, N. *Talanta* **1987**, *34*, 739.
(5) Leonhardt, H.; Gordon, L.; Livingston, R. *J. Phys. Chem.* **1971**, *75*, 245.
(6) Yguerabide, J. *Methods Enzymol.* **1972**, *26*, 798.
(7) (a) Marquardt, D. W. *J. Soc. Ind. Appl. Math.* **1963**, *11*, 431. (b) Yguerabide, J.; Yguerabide, E. *Optical Techniques in Biological Research*; Rousseau, D. L., Ed.; Academic Press: San Diego, 1984; Chapter 4.
(8) (a) Beechem, J. M.; Ameloot, M.; Brand, L. *Chem. Phys. Lett.* **1985**, *120*, 466. (b) Beechem, J. M. *Methods Enzymol.* **1992**, *210*, 37.
(9) Yguerabide, J.; Burton, M. *J. Chem. Phys.* **1962**, *37*, 1757.
(10) Durbin, J.; Watson, G. S. *Biometrika* **1951**, *38*, 159.
(11) (a) Rozwadowski, M. *Acta Phys. Pol.* **1961**, *20*, 1005. (b) Ware, W. R.; Baldwin, B. A. *J. Chem. Phys.* **1964**, *40*, 1703. (c) Flamigni, L. *J. Phys. Chem.* **1993**, *97*, 9566.